# An Optimal Driving Force for Converting Excitons into Free Carriers in Excitonic Solar Cells

**8 AUTHORS**, INCLUDING:

Alexander W. Hains
MicroLink Devices, Inc.
**15** PUBLICATIONS **1,594** CITATIONS

SEE PROFILE

James Whitaker
**12** PUBLICATIONS **156** CITATIONS

SEE PROFILE

Olga V. Boltalina
Colorado State University
**268** PUBLICATIONS **4,252** CITATIONS

SEE PROFILE

# An Optimal Driving Force for Converting Excitons into Free Carriers in Excitonic Solar Cells

David C. Coffey,[†] Bryon W. Larson,[‡] Alexander W. Hains,[†] James B. Whitaker,[‡] Nikos Kopidakis,[†] Olga V. Boltalina,[‡] Steven H. Strauss,[‡] and Garry Rumbles*[,†,§]

[†]National Renewable Energy Laboratory, 15013 Denver West Parkway, Golden, Colorado 80401, United States
[‡]Department of Chemistry, Colorado State University, Fort Collins, Colorado 80523, United States
[§]Department of Chemistry and Biochemistry, University of Colorado, Boulder, Colorado 80309, United States

Ⓢ Supporting Information

**ABSTRACT:** A general but limiting characteristic in excitonic photovoltaics is that a portion of the incident photon energy appears necessary for converting excitons into electrical charges, resulting in a loss of efficiency. Currently, the mechanism underlying this process is unclear. Here, we describe the development of an experimental method for measuring charge creation yields in organic solar cell materials. We use this method to examine a series of conjugated polymer:fullerene blend films and observe two unexpected features: the existence of an optimal driving force and a loss in conversion efficiency if this force is exceeded. These observations have implications for the design of excitonic photovoltaic devices and can be explained by a simple Marcus formulation that introduces the importance of reorganization energy.
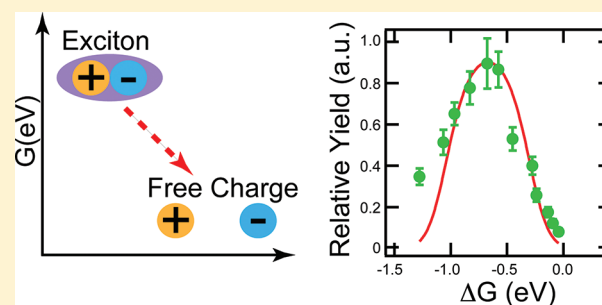
## ■ INTRODUCTION

Photoinduced electron transfer (PET) is a fundamental process in photochemistry and photophysics and is a key step in the operation of excitonic solar cells.[1−17] In many promising photovoltaic materials with low dielectric constants, light absorption does not necessarily induce PET and the creation of free charges but rather generates bound excitons. Excitonic solar cells are designed to ensure that the overall PET process results in the conversion of these excitons into free electrons and holes, as shown in Figure 1.[5−7] This is commonly achieved by combining donor and acceptor materials to create type II heterojunctions that establish a sufficient driving force to ensure PET. However, energy is lost when setting up this driving force. In photosynthetic systems, this loss might be as little as 0.2 eV.[8,9] In today's best excitonic solar cells, the quantum yields for converting photons into free charge can be nearly 100%, but to achieve this efficiency, it is common to lose up to 1.0 eV. Some of this lost voltage has been attributed to band bending (ca. 0.35 eV), finite widths in the density of states (ca. 0.1 eV), or poor band alignment, but an important piece (0.3−0.7 eV) is seemingly required to drive charge separation.[5−7,10−16,18] Currently, the mechanism underlying this later energy loss is unclear, and no consensus exists about how this loss might be mitigated for the next generation of excitonic solar cells.

Systematically testing PET in excitonic solar cells—systematically varying energy levels as the initial and final states are probed—requires overcoming numerous challenges. First, the
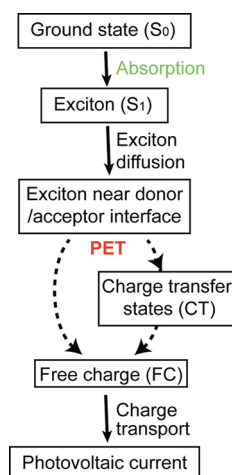


**Figure 1.** Scheme describing the multistep process an excitonic solar cell undertakes to convert photons into electrical current. The progression through intermediate CT states and the energy necessary to drive the overall process are still subjects of study.

final state is composed of separated charge, the existence of which is difficult to probe and thus is often only indirectly inferred from fluorescence, optical absorption, or device voltage

measurements.[5,6,11] Second, the sequence for converting light into electricity requires several steps (see Figure 1): photon absorption, exciton generation, exciton diffusion to a donor/acceptor interface, PET [possibly through an intermediate charge transfer (CT) state],[5−7,10−14,19] and charge transport to external contacts; so, extracting information specific to PET is often problematic.[7,16] Third, it has proved difficult to experimentally correlate short-lived CT states with overall charge creation efficiency. Fourth, absorption can occur in either the acceptor or the donor, leading to two distinct photophysical pathways. Fifth, each fundamental process is complicated by numerous extrinsic factors: (1) processes that are nonlinear with light intensity such as recombination, (2) varying mobilities, and (3) heterogeneous donor/acceptor mixing.[20−22] Sixth, systematically varying the energy-driving PET requires synthesizing multiple, interchangeable donor/acceptor molecules that do not simultaneously alter any of the factors listed above, an achievement that is rarely attained.[5−7,10,11,23]

Below, we describe a new type of experimental method that allows us to overcome each of these challenges. In short, three strategies allow us to observe intrinsic charge creation in photovoltaic films: (1) we probe our samples using time-resolved microwave conductivity (TRMC), directly measuring free charge and removing the importance of charge transport and external contacts; (2) we fabricate our samples in a "dilute regime" and only excite the diluted acceptor molecules, reducing the complications associated with exciton diffusion, unknown mobilities, and varying morphology; and (3) we use a series of interchangeable acceptor molecules, modified fullerenes, to systematically vary the Gibbs energy change driving the entire charge creation process (also allowing us to proceed without knowing the energy of any intermediate CT states). In the remainder of this paper, we will describe each of these strategies in detail, apply them to a series of donor/acceptor films, discuss the importance of the experimental results for designing improved excitonic solar cells, and, finally, compare the results with the predictions of PET theories, including Marcus Theory.

## ■ EXPERIMENTAL SECTION

Figure 2 summarizes a set of experiments that lead to the measurement of intrinsic charge creation yields in polymer/fullerene excitonic photovoltaic films. First, a series of polymer/fullerene, F8T2/PC$_{70}$BM films (see Figure 2b inset for structures; see Tables 1 and 2 for chemical names) are fabricated on quartz substrates with varying relative concentrations. This particular donor/acceptor combination produces a type II heterojunction suitable for charge generation. The laser wavelength used in these experiments, 570 nm, is chosen to selectively illuminate the fullerene molecules and not the polymer (Figure 2b, note that this is the less typical pathway for absorption in standard polymer/fullerene devices). Figure 2c plots several example time-dependent photoconductance traces for this series as measured with TRMC. The details of performing TRMC experiments and analysis are reported in the Methods. Briefly, however, samples are placed in the TRMC resonant microwave chamber where the transient change in microwave power due to a 5 ns laser pulse is proportional to the transient change in the sample's photoconductance.[22,24−30] With TRMC, we look at the generation and decay of photoinduced charge, assuming that the change in photoconductance equals $IA\Delta(\phi\Sigma\mu)$, where $I$ is the illumination
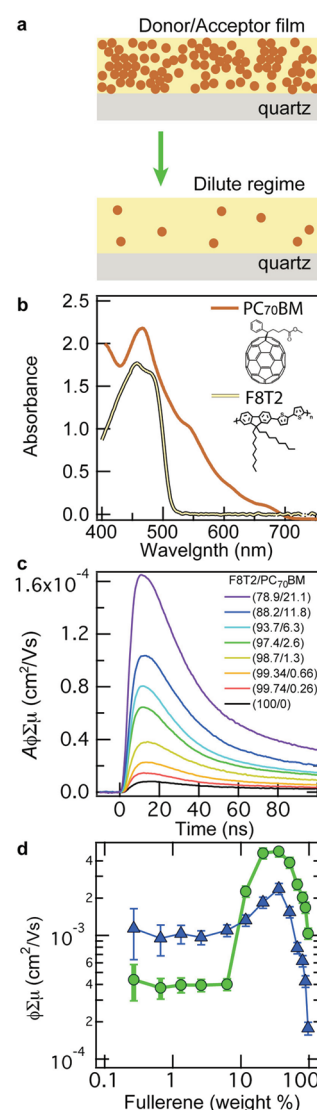


**Figure 2.** Measuring intrinsic charge creation yields in the dilute regime. A series of F8T2/PC$_{70}$BM films were fabricated with varying relative concentration, focusing on the dilute regime of little acceptor. (a) A depiction of a film in the dilute acceptor regime, (b) absorbance spectra of F8T2 (yellow trace) and PC$_{70}$BM (brown trace) (note, 570 nm TRMC illumination), (c) characteristic TRMC transients for F8T2/PC$_{70}$BM films (key shows wt ratios), (d) F8T2/fullerene peak photoconductivity as a function of PC$_{70}$BM weight percentage (green circles) and C$_{60}$(CF$_3$)$_6$-2 wt % age (blue triangles). The error bars are standard errors calculated as described in the Methods.

intensity, $A$ is the sample absorbance, $\phi$ is the charge creation yield, and $\Sigma\mu$ is the sum of hole and electron mobilities. In this study, we only look at the initial peak height, not the decay, and interpret it to be proportional to the peak photoconductivity of the sample (equal to the product of the free charge yields and their GHz mobility). Previous studies have shown that TRMC is sensitive to both mobile electrons in aggregated fullerene domains and mobile holes in polymer domains (in our final measurements, as will be discussed later, we are only sensitive to mobile holes in the polymer).[22,24−26,28−30] In Figure 2c, it is sufficient to observe that the peaks of the photoconductance traces trend higher as increasing amounts of fullerene are added, coincident with the increased photovoltaic activity expected in devices containing the same blended films.

## ■ METHODS

**Sample Fabrication and Characterization.** Sample films were fabricated by drop-casting a solution of polymer/fullerene onto a precleaned quartz substrate in air. The solutions were prepared by dissolving polymer and fullerene separately into chloroform/chlorobenzene (90/10 by volume) for stock solutions. These solutions were paired with additional pristine chloroform/chlorobenzene solution to make drop-casting solutions with a polymer concentration of 5 mg/mL and a varying fullerene concentration. The film absorption was measured with a Shimadzu integrating sphere at multiple locations covering the entire film to account for potential variations in film thickness.

Polymers were purchased from American Dye Source (F8T2), H. W. Sands Corporation (F8), and Aldrich (F8BT). The perfluoroalkyl fullerenes were synthesized, and their isomers were purified by our team as described previously.[23] The remaining fullerenes were purchased from Nano-C ($PC_{60}BM$ and $PC_{70}BM$) Solenne (bis-$PC_{60}BM$) or provided by Plextronics ($IC_{60}MA$ and $IC_{60}BA$) and used as received. Purchased fullerenes had a stated purity great than 99%. Fullerenes synthesized by our team were characterized by HPLC, showing a purity greater than 95% for all samples except for 85% purity for $C_{60}(CF_3)_{10}$-1. Fullerene exciton energies were determined by optical spectroscopy as described in the Supporting Information.

**Cyclic Voltammetry (CV).** CV measurements for the fullerenes were measured relative to each other as previously described.[23] The electron affinity, EA, for $PC_{60}BM$ was pegged at 4.2 eV, and the other EA values were determined relative to this value using the CV measured $E_{1/2}$ reduction values. We note that while changes in reduction potential are not guaranteed to reflect identical changes in EA, density functional theory lowest unoccupied molecular orbital (DFT LUMO) calculations by Popov et al. support overall correlations found for the fullerene materials used here.[23] CV measurements for the polymers were performed on films using scan rates of 10−100 mV/s with either Pt or glassy carbon working electrodes in acetonitrile (Aldrich, 99.9%) with 0.1 M $Bu_4N^+PF_6^-$ (recrystallized from ethanol) as the electrolyte.[31,32] A platinum counterelectrode and a Ag/AgCl reference electrode were employed, the Fc/Fc$^+$ couple was used to verify the validity of results, and the results were converted to the standard calomel electrode (SCE) scale using $E^0_{Ag/AgCl}$ = −0.044 V vs SCE. The measured oxidation potentials were converted to the vacuum scale to determine the IPs using the following relationships in which $e$ is the electron charge:

$$E^{onset}_{ox\ vs\ SCE} + 0.24V = E^{onset}_{ox\ vs\ NHE}$$

$$4.5eV + eE^{onset}_{ox\ vs\ NHE} = E_{IP}$$

The random error that we associate with CV measurements for the fullerenes has previously been estimated at 10 meV.[23] We estimate the random error for the polymer values to be 50 meV. However, we note that CV measurements also possess a large systematic uncertainty, and different analysis techniques can return values that vary greatly.[32] This methodological uncertainty does not affect the validity of our analysis because we use self-consistent relative values, but they would be important when trying to quantify the absolute energy of the final free charge state.

**TRMC Measurements.** TRMC measurement details have been described previously.[22,24,25] Measurements were made in air on the same day as sample fabrication. Select measurements made in nitrogen showed no difference in the resulting values. To determine film photoconductivities, the following procedure is followed: (1) TRMC data of the sample series are taken over a range of illumination intensities to ensure that the response is linearly correlated with light intensity, (2) these traces are fit to a triple exponential function and deconvoluted from the ca. 7 ns cavity response,[33] (3) the small background signal measured for pristine F8T2 and quartz (Figure 2b black trace) is subtracted from the resulting signal, and (4) the resulting peak value is normalized by the film absorption. Examples for each step are given in the Supporting Information.

The photoconductivity measurement errors in these experiments are dominated by errors inherent in measuring the optical absorption and from errors associated with sample-to-sample variation. The errors in Figure 2 are estimated by (1) measuring the photoconductance multiple times for several samples fabricated in an identical fashion and extracting a standard deviation (10% standard deviation) and (2) by measuring the optical absorption multiple times for the same sample and extracting a standard deviation (0.05% absorption standard deviation).

## ■ RESULTS AND DISCUSSION

**Measuring Charge Creation Yields in the Dilute Regime.** The green trace in Figure 2d plots the peak photoconductivity of the F8T2/$PC_{70}BM$ series as a function of fullerene concentration and is a key plot in this paper. Each point in this trace corresponds to the peak of a photoconductance trace as shown in Figure 2c, normalized by the film's optical absorption and the pristine F8T2 film's background signal (see Methods for details). As is expected in donor/acceptor systems, the photoconductivity increases with increasing acceptor concentration, reaching a peak value near 30% fullerene.[20,25] However, in the "dilute regime" below ca. 6% fullerene, a regime that is rarely considered in experiments associated with organic photovoltaics, the photoconductivity is relatively constant.

A constant photoconductivity as a function of acceptor concentration in the dilute regime has important consequences, including indicating (1) an absence of changing extrinsic factors such as changing morphology or fullerene aggregation, (2) a constant mobility, and, most importantly, (3) a constant yield. Such results can be understood by appreciating the morphology specific to the dilute regime. First, the constant photoconductivity suggests a morphology of fullerenes isolated in pristine polymer (Figure 2a). Previous TRMC studies have demonstrated that fullerene aggregation enables electronic coupling between the fullerenes that leads to an increase in photoconductivity, not a constant photoconductivity.[22,24−26,28] In the idealized dilute regime discussed here where such couplings are not generated, the difference between higher and lower fullerene concentration will only correspond to differences in the extent of fullerene isolation. In all cases, the fullerene molecules are isolated. As such, for the remainder of this paper, we presume that a constant photoconductivity indicates minimal aggregation. Second, with such a morphology and an optically transparent polymer, excitons are created solely on the fullerene molecules and thus are created already at the charge creation interface; therefore, exciton diffusion becomes unimportant (at 570 nm, the fullerenes are the dominant

**Table 1. Characteristic Data for Measured Fullerene Acceptor Molecules Paired with F8T2[23,31,32]**

| fullerene | | sidegroup type | $E_{Initial}$[a] ($E_{Exciton}$) (eV) | fullerene EA (eV) | F8T2 IP (eV) | $E_{Final}$[b] (eV) | $\Delta G$[c] (eV) |
|---|---|---|---|---|---|---|---|
| $IC_{60}BA$ | indene-$C_{60}$ bis-adduct | | 1.72 | 4.04 | 5.72 | 1.68 | -0.04 |
| $IC_{60}MA$ | indene-$C_{60}$ mono-adduct | | 1.73 | 4.08 | 5.72 | 1.64 | -0.09 |
| bis-$PC_{60}BM$ | Bis(1-[3-(methoxycarbonyl)propyl]-1-phenyl)-[6.6]$C_{62}$ | | 1.75 | 4.11 | 5.72 | 1.61 | -0.14 |
| $PC_{60}BM$ | [6,6]-phenyl-$C_{61}$-butyric acid methyl ester | | 1.76 | 4.20 | 5.72 | 1.52 | -0.24 |
| $PC_{70}BM$ | [6,6]-phenyl-$C_{71}$-butyric acid methyl ester | | 1.78 | 4.21 | 5.72 | 1.51 | -0.27 |
| $C_{60}(CF_3)_2$-1 | 1,7-$C_{60}(CF_3)_2$ | | 1.77 | 4.43 | 5.72 | 1.29 | -0.48 |
| $C_{60}(CF_3)_4$-1 | 1,6,11,18-$C_{60}(CF_3)_4$ | | 1.84 | 4.46 | 5.72 | 1.26 | -0.58 |
| $C_{60}(CF_3)_6$-2 | 1,6,9,12,15,18-$C_{60}(CF_3)_6$ | | 2.18 | 4.22 | 5.72 | 1.50 | -0.67 |
| $C_{60}(CF_3)_6$-1 | 1,6,11,18,24,27-$C_{60}(CF_3)_6$ | | 2.00 | 4.55 | 5.72 | 1.17 | -0.83 |
| $C_{60}(CF_3)_8$-1 | 1,6,11,16,18,24,27,36-$C_{60}(CF_3)_8$ | | 2.07 | 4.62 | 5.72 | 1.10 | -0.97 |
| $C_{60}(CF_3)_{10}$-2 | 1,6,11,16,18,26,36,44,48,58-$C_{60}(CF_3)_{10}$ | | 2.18 | 4.61 | 5.72 | 1.11 | -1.06 |
| $C_{60}(CF_3)_{10}$-1 | 1,6,11,16,18,24,27,36,41,57-$C_{60}(CF_3)_{10}$ | | 2.14 | 4.86 | 5.72 | 0.86 | -1.28 |

[a]The initial energy ($E_{exciton}$) is the exciton energy found in isolated fullerenes as measured by optical spectroscopy. [b]The final energy (free carrier energy) is given as the difference between the fullerene EA and the polymer ionization potential (IP), which are, in turn, estimated from CV measurements (see the Methods). [c]The change in Gibbs' energy, $\Delta G$, is tabulated according to eq 1.

absorbing component). Third, electrons are generated on the isolated fullerenes and thus do not exhibit a significant high-frequency, GHz mobility. Such a dependence of electron mobility on fullerene aggregation has been previously measured.[25] The detected high-frequency mobility is dominated by the hole mobility in the polymer, which does not change through the dilute regime.[29,30,34] Taken together, these points explain why a constant yield can be found through the dilute regime: excitons are generated on isolated fullerenes, these excitons do not have to diffuse, and these excitons are dissociated with the electrons remaining on the fullerenes and the holes free to move through the polymer. Most significantly, these trends reveal the development of the long-desired experimental capability of measuring an intrinsic yield, a tool that enables the fundamental study that we describe below.

The blue trace in Figure 2d plots the photoconductivity as a function of fullerene weight percent for a second fullerene acceptor series, $C_{60}(CF_3)_6$-2.[23] Critically, the photoconductivity is again constant in the dilute regime below ca. 6% fullerene. Once more, this implies a constant yield through the dilute regime. Comparing the blue and green traces in the dilute regime, the shared polymer mobility between the two series implies that the factor of 3 increase in the photoconductivity of the $C_{60}(CF_3)_6$-2 series (blue trace) compared to the $PC_{70}BM$ series (green trace) corresponds to a factor of 3 increase in the intrinsic yield. We note that while $PC_{70}BM$ has a larger optical cross-section than $C_{60}(CF_3)_6$-2, which leads to a greater photoconductance, the data in Figure 2d are normalized by absorption to give photoconductivity. Consequently, Figure 2d demonstrates a method for comparing yields as the acceptor species is changed. This method was repeated below for the series of fullerenes shown in Table 1.

**Measurement and Analysis of Carrier Yield Versus $\Delta G$.** Table 1 lists the dozen fullerenes used in these experiments to systematically vary the Gibbs energy driving force for electron transfer. When the fullerene/polymer films engage in PET, this change in Gibbs energy, $\Delta G$, can be understood to good approximation as the change in energy between the initial exciton energy, $E_{exciton}$, and the final hole/electron energy, $E_{final}$:

$$\Delta G = E_{final} - E_{initial}$$

$$\text{i.e. } \Delta G = IP_D - EA_A - E_{exciton} \qquad (1)$$

where $IP_D$ is the ionization potential of the donor and $EA_A$ is the EA of the acceptor. We do not believe that other factors, such as entropic terms, are likely to vary significantly within our sample set, and as such, they are not included in the $\Delta G$ analysis that follows. $E_{exciton}$ values were measured by optical spectroscopy. To estimate values for $IP_D$ and $EA_A$, as given in Table 1, the oxidation and reduction potentials were measured with CV, as described in the Methods section above, with a broader discussion provided in the Supporting Information.

Figure 3a plots the intrinsic yield of charge creation versus the change in Gibb's energy for each fullerene combined with F8T2 as measured in the dilute regime at 570 nm. Each data point corresponds to the constant photoconductivity value as shown in Figure 2d (ca. 4% fullerene by weight). We note that while fullerene aggregation at such concentrations has been observed in poly(3-hexylthiophene), where fullerene miscibility is low,[22] we assert that such a concentration in polyfluorene type polymers resides in the dilute regime, similar to MDMO-PPV,[26] indicating minimal aggregation effects (see the Supporting Information, Figure S6). Thus, as the mobility in each specific polymer sample is the same (the hole mobility of F8T2), the relative differences between the high-dilution values in Figure 3a correspond to relative differences in the intrinsic yield of separated carriers.

To expand our data set, we have repeated these experiments with two other polymers, F8BT and F8, in the same polyfluorene family as F8T2 (see Table 2). Figure 3b,c show equivalent data for F8BT and F8, respectively. Before interpreting these data, it is useful to recognize two important experimental details. First, the $\Delta G$ values for each data series are shifted between polymer series because the ionization potential for each polymer varies (F8T2 = −5.7 V, F8 = −5.9 V, and F8BT = −6.1 V). Thus, while the order and spacing of the data points remain constant and correspond to the same fullerene molecules, the absolute $\Delta G$ values are shifted. Second, the yield values are only given as relative yields because it is the photoconductivity that is measured, and 10 GHz hole mobilities have not been determined for these polymers.
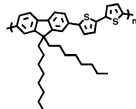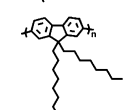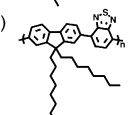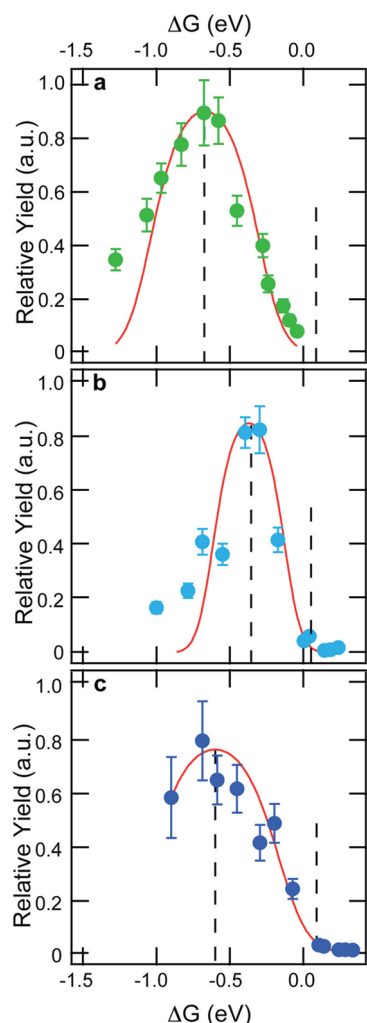
**Figure 3.** Relative yield vs $\Delta G$ plotted for three polymers. Each plot corresponds to a series of films with a dozen fullerenes and (a) F8T2, (b) F8, and (c) F8BT. The order of the data points corresponds to fullerenes in the same order as given in Table 1. The error bars represent standard errors calculated as described in the Methods and are most impacted by sample-to-sample variation and the accuracy of measuring sample absorptions. The solid red lines correspond to fits based on eqs 1−3. The dashed black lines mark the "turn-on" regime from zero yield to peak yield.

Two key observations can be gleaned from the data in Figure 3, the implications of which lead to the primary conclusions of

**Table 2. Polymer Abbreviation, Name, Structure, and Ionization Potential Approximated from CV Measurements**

| | | |
|---|---|---|
| **F8T2** | Poly(9,9-dioctylfluorene-*alt*-bithiophene) | |
| | IP = 5.7 eV | |
| **F8** | Poly(9,9-dioctylfluorene) | |
| | IP = 5.9 eV | |
| **F8BT** | Poly(9,9-dioctylfluorene-*alt*-benzothiadiazole) | |
| | IP = 6.1 eV | |

this paper. First, the carrier yield values for each series increase gradually from a near-zero value near $\Delta G = 0$, to a peak value, and then begin to decrease with further increase in the driving force. This inversion is not observed fully in F8BT because the deep ionization potential of F8BT, $IP_D$, means sufficiently exergonic $\Delta G$ values are not attained. Second, the width of the normal/inverted region in the F8 series is narrower than the width of the same features in the F8T2 series. In F8, the Gibbs energy required to reach a peak carrier yield proceeds over a range of $0.4 \pm 0.1$ eV, whereas in F8T2, this turn-on proceeds over $0.8 \pm 0.1$ eV.

Before interpreting these trends, we first consider whether the turn-on and inverted regions are intrinsic to the materials or extrinsic artifacts of the experiment. To begin, it is important to recognize that charge creation yields depend on both the rate constant for the free-charge creation process and the competing rate constant for other radiative and nonradiative loss pathways for the exciton. Loss mechanisms for the photogenerated carriers, such as recombination and trapping, can be seen from the long-lived transients in Figure 2c to be slow with respect to the charge-generating step. If the yields measured in Figure 3 are dominated by a single rate-limiting step, $k_{CC}$, the charge creation yield can be written:

$$\text{yield}_{CC} = \frac{k_{CC}}{k_{CC} + k_{\text{losses}}} \tag{2}$$

where $k_{\text{losses}}$ represents the total rate of all of the loss pathways. Of primary consideration is the possibility that when modifying the fullerene side group (adduct) to change the $\Delta G$ force driving charge creation, other factors affecting $k_{\text{losses}}$ might simultaneously change. Examples include (1) the accessibility of a loss pathway like fluorescence, (2) the fullerene self-electron transfer rate constant, which is contained within $k_{CC}$, or (3) the insulating barrier that partially surrounds the $C_{60}$ molecule. In considering all such possibilities, however, it is important to observe that the fullerenes corresponding to the normal region in F8BT correspond to the inverted region in F8T2 (the order of fullerenes in Figure 3a−c remains constant). This shift is counter to what one would expect if the particular side groups and not $\Delta G$ was the key factor determining the yield. This indicates that $\Delta G$ is the dominant factor that determines the yield in these experiments, and the yields measured for Figure 3 are truly indicative of intrinsic charge creation. While CT states are often considered to be a precursor to charge creation, we note that these measurements cannot detect these intermediate states and are sensitive only to the overall creation yields of separated charges.

Assuming that the data are truly indicative of the rate-limiting charge creation step, the trends found in Figure 3 tell a clear story of the charge creation step found in excitonic photovoltaic systems: (1) charge creation yield rises gradually as the driving force, $|\Delta G|$, is increased from zero, (2) peak efficiency requires a significant driving force (e.g., 0.8 and 0.4 eV for F8T2/fullerenes and F8/fullerenes, respectively), (3) greater driving forces do not continue to promote charge creation but rather push the system into an inverted region, and (4) the $\Delta G$ value that optimizes the yield is specific to the particular "donor" polymer. Taken together, these features emphasize that for efficient excitonic photovoltaic systems, the donor and acceptor *combination* must be chosen properly. While such knowledge is often inferred through empirical studies, Figure 3 explicitly maps this dependence. For a given solar cell, $IP_D$, $EA_A$, and

$E_{exciton}$ must be balanced precisely to optimize the charge creation efficiency.

While these conclusions are only demonstrated experimentally for this specific set of materials and for low fullerene concentration, these simple architectures embody the heart of more complicated devices—donor and acceptor materials mixed in a solid-state film—and their conclusions should inform numerous systems. The requirement of balance found in these simple systems suggests a set of rules for the field of excitonic photovoltaics: (1) no single, prototypical acceptor (e.g., $PC_{60}BM$) can be expected to adequately test the worth of every newly synthesized donor species, (2) analogously, no single, prototypical donor (e.g., P3HT) can be expected to adequately test the worth of every newly synthesized acceptor, (3) a system optimized for efficient charge creation when excitons are photogenerated in the donor will not necessarily be optimized for excitons photogenerated in the acceptor because the exciton energies, $E_{exciton}$, will be different, and (4) different material systems will require a range of optimal driving forces that will result in a range of open-circuit voltages.

While these rules can be used to better understand excitonic photovoltaics, the fourth rule in particular presents an opportunity. Specifically, the difference in the optimal driving force found between the F8 and the F8T2 series highlights that the optimal driving force varies from system to system and, as such, might be intelligently minimized in other photovoltaic systems. In the remainder of this paper, we discuss a mechanistic picture that suggests a distinct pathway toward this tantalizing goal.

**Marcus Theory as a Potential Way To Describe Charge Creation.** To finish, we provide a short discussion on what these experiments might imply about the mechanism of charge creation in excitonic photovoltaics. Multiple processes and routes have been postulated as necessary to explain charge creation in excitonic solar cells, including intermediate CT states, thermally excited CT states, triplet excitonic states, charge trapping, Coulombic binding, Onsager Theory, and Marcus Theory.[5−8,10,11,14,16,35,36] While the trends in Figure 3 discussed above do not preclude a composite mechanism based on some entangled competition between these possibilities, Marcus Theory arises as an intriguing possibility to describe charge creation in these systems because it is unique in providing a simple justification for the observed inverted region.

Marcus' theory is the fundamental theory for understanding long-range electron transfer rates in molecular systems that are not diffusion limited.[37−40] While confirmed experimentally for recombination processes in solution 25 years ago, unambiguously observing its predictions for nonemissive PET has remained an elusive goal.[40−43] Figure 4a depicts a hypothetical Marcus Theory picture for PET in exciton photovoltaics, where the electron transition from an initial state to a final state depends on both the change in Gibbs energy, $\Delta G$, and the reorganization energy, $\lambda$, associated with the energy needed to arrange the initial state into the configuration of the final state.

In Marcus Theory, approximations for the free energy surfaces lead to the prediction of an electron transfer rate constant:

$$k_{PET} = A_{PET}e^{-(\Delta G - \lambda)^2/4\lambda RT} \qquad (3)$$

This rate equation predicts a "normal region" for smaller exergonic changes and an "inverted region" for large exergonic
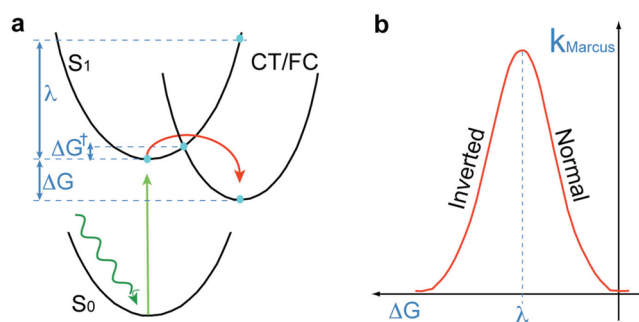


**Figure 4.** PET and Marcus Theory. (a) A Marcus Theory representation of the PET process, including the change in Gibb's energy, $\Delta G$, and the reorganization energy, $\lambda$. The necessity of reorganization introduces an activation barrier, $\Delta G^{\dagger}$, that the system must pass over if electron transfer is to occur. (b) Marcus Theory predicts a Gaussian dependence of the rate constant with a characteristic inverted region, with the peak location and width being determined by the reorganization energy.

changes where the rate decreases with increasing $|\Delta G|$ (Figure 4b).

These simple predictions of Marcus Theory are applicable to our data if the charge creation rate constant of eq 2, $k_{CC}$, is dominated by the rate constant for PET, $k_{PET}$, and if $k_{losses}$ are correspondingly small. To provide a first test of the applicability of Marcus Theory, eqs 1−3 were used to fit the data in Figure 3 ($k_{losses}$ is held globally constant at a value of $0.33*A_{PET}$, where $A_{PET}$ is from eq 3. The prefactor of 0.33 is chosen such that the yield approaches 0.67, a value representative of polymer/fullerene systems) to produce the red traces. Indeed, these fits capture the previously discussed key trends and suggest that Marcus Theory might be used to understand the charge creation process (we note that explicitly testing the numerous process rates, beyond what has already been discussed, is beyond the scope of this initial work, and we introduce this Marcus Theory-based analysis as a preliminary but intriguing hypothesis).

Assuming the suitability of a Marcus Theory-based analysis, the fits in Figure 3 show two important features. First, the width of the F8 charge creation curve is narrower than the F8T2 curve. Second, the peak yields are found at different $\Delta G$ values. Both of these differences correlate through eq 3 to a change in reorganization energy;[6,44] a simple change in reorganization energy from F8T2 to F8 of 0.8 to 0.4 eV used in the Figure 3 fits accounts for both the shift in peak position and the width. To understand these differences and the apparent changes in reorganization energy between polymers, we speculate that the relatively flexible thiophene units within F8T2 probably lead to a larger reorganization energy than the relatively rigid polyfluorene monomers within F8. Full reorganization energies have not been measured for the polymer:fullerene pairings measured here but would be expected to be in the range of 0.3−0.9 eV, consistent with the fits.[8] In sum, Marcus Theory, at the least, can potentially provide an intriguing description of the observations of the turn-on region, the inverted region, the variation in curve width, and the variation in peak position.

The agreement between our data and these simple predictions suggest that Marcus Theory might be employed to understand charge generation more broadly in excitonic solar cells. When applied to the mystery of why 0.3−1.0 eV of energy is seemingly required to drive charge creation, this

picture of Marcus Theory says that this energy is required to spur reorganization. Of course, maximizing $k_{PET}$ and minimizing competing loss processes ($k_{losses}$) will also remain important, but this picture says that to ensure good charge creations yields, the acceptor and donor materials must be carefully chosen to balance $\Delta G$ and $\lambda$. Indeed, the failure of many of the enormous number of seemingly promising donor/acceptor pairs might be accounted for by a poor balance of $\Delta G$ and $\lambda$. Furthermore, this picture suggests that a key route for improving future excitonic solar cells might be to reduce the reorganization energy inherent in PET.

## CONCLUSION

In conclusion, we have developed a method for measuring intrinsic charge creation yields in excitonic photovoltaic films. Applied to a series of polymer/fullerene films, we observe that a significant amount of energy is required to drive charge creation and that excess driving force leads to an inverted region. Furthermore, we show that the energy required to drive charge creation depends on the particular donor host. These observations indicate that the energy that has seemingly been required to drive charge creation in excitonic photovoltaics is indeed an intrinsic requirement but that this energy loss might be minimized through an intelligent pairing of donors and acceptors. Furthermore, we discuss how these experimental observations can possibly be understood through a simple version of Marcus Theory. A key practical conclusion of this paper is that a vital pathway for improving excitonic solar cells will be to reduce the energy required to drive PET, possibly by reducing the associated reorganization energy. Such a strategy has been hypothesized as a possibility before and is apparently utilized by the photosynthetic apparatus.[6,8,45] This work demonstrates the fundamental practicality and importance of such a strategy for artificial, man-made systems.

## ASSOCIATED CONTENT

**Ⓢ Supporting Information**

More thorough description of the experimental procedures, including TMRC measurements, data fitting, and optical measurements. This material is available free of charge via the Internet at http://pubs.acs.org.

## AUTHOR INFORMATION

**Corresponding Author**
*E-mail: Garry.Rumbles@nrel.gov.

**Notes**
The authors declare no competing financial interest.

## ACKNOWLEDGMENTS

## REFERENCES

(1) Gregg, B. A. *MRS Bull.* **2005**, *30*, 20−22.
(2) Nelson, J. *Science* **2001**, *293*, 1059−1060.
(3) Park, S. H.; Roy, A.; Beaupre, S.; Cho, S.; Coates, N.; Moon, J. S.; Moses, D.; Leclerc, M.; Lee, K.; Heeger, A. J. *Nat. Photonics* **2009**, *3*, 297−303.
(4) McGehee, M. D. *Nat. Photonics* **2009**, *3*, 250−252.
(5) Ohkita, H.; Cook, S.; Astuti, Y.; Duffy, W.; Tierney, S.; Zhang, W.; Heeney, M.; McCulloch, I.; Nelson, J.; Bradley, D. C. C.; Durrant, J. R. *J. Am. Chem. Soc.* **2008**, *130*, 3030−3042.
(6) Clarke, T. M.; Durrant, J. R. *Chem. Rev.* **2010**, *110*, 6736−6767.
(7) Bredas, J. L.; Norton, J. E.; Cornil, J.; Coropceanu, V. *Acc. Chem. Res.* **2009**, *42*, 1691−1699.
(8) Imahori, H.; Tkachenko, N. V.; Vehmanen, V.; Tamaki, K.; Lemmetyinen, H.; Sakata, Y.; Fukuzumi, S. *J. Phys. Chem. A* **2001**, *105*, 1750−1756.
(9) Nelson, N.; Ben-Shem, A. *Nat. Rev. Mol. Cell Biol.* **2005**, *6*, 818−818.
(10) Vandewal, K.; Gadisa, A.; Oosterbaan, W. D.; Bertho, S.; Banishoeib, F.; Van Severen, I.; Lutsen, L.; Cleij, T. J.; Vanderzande, D.; Manca, J. V. *Adv. Funct. Mater.* **2008**, *18*, 2064−2070.
(11) Rand, B. P.; Burk, D. P.; Forrest, S. R. *Phys. Rev. B* **2007**, *75*, 115327.
(12) Muntwiler, M.; Yang, Q.; Tisdale, W. A.; Zhu, X.-Y. *Phys. Rev. Lett.* **2008**, *101*, 196403.
(13) Veldman, D.; Meskers, S. C. J.; Janssen, R. A. *Adv. Funct. Mater.* **2009**, *19*, 1939−1948.
(14) Bredas, J. L.; Beljonne, J. E.; Coropceanu, V.; Cornil, J. *Chem. Rev.* **2004**, *104*, 4971−5003.
(15) Scharber, M. C.; Muhlbacher, D.; Koppe, M.; Denk, P.; Waldauf, C.; Heeger, A. J.; Brabec, C. J. *Adv. Mater.* **2006**, *18*, 789−794.
(16) Nelson, J.; Kirkpatrick, J.; Ravirajan, P. *Phys. Rev. B* **2004**, *69*, 035337.
(17) McMahon, D. P.; Cheung, D. L.; Troisi, A. *J. Phys. Chem. Lett.* **2011**, *2*, 2737−2741.
(18) Mihailetchi, V. D.; Blom, P. W. M.; Hummelen, J. C.; Rispens, M. T. *J. Appl. Phys.* **2003**, *94*, 6849−6854.
(19) McMahon, D. P.; Cheung, D. L.; Troisi, A. *J. Phys. Chem. Lett.* **2011**, *2*, 2737−2741.
(20) Arias, A. C.; MacKenzie, J. D.; Stevenson, R.; Halls, J. J. M.; Inbasekaran, M.; Woo, E. P.; Richards, D.; Friend, R. H. *Macromolecules* **2001**, *34*, 6005−6013.
(21) Coffey, D. C.; Reid, O. G.; Rodovsky, D. B.; Bartholomew, G. P.; Ginger, D. S. *Nano Lett.* **2007**, *7*, 738−744.
(22) Ferguson, A. J.; Kopidakis, N.; Shaheen, S. E.; Rumbles, G. *J. Phys. Chem. C* **2008**, *112*, 9865−9871.
(23) Popov, A. A.; Kareev, I. E.; Shustova, N. B.; Stukalin, E. B.; Lebedkin, S. F.; Seppelt, K.; Strauss, S. H.; Boltalina, O. V.; Dunsch, L. *J. Am. Chem. Soc.* **2007**, *129*, 11551−11568.
(24) Kroeze, J. E.; Savenije, T. J.; Vermeulen, M. J. W.; Warman, J. M. *J. Phys. Chem. B* **2003**, *107*, 7696−7705.
(25) Savenije, T. J.; Kroeze, J. E.; Wienk, M. M.; Kroon, J. M.; Warman, J. M. *Phys. Rev. B* **2004**, *69*, 155205.
(26) Dicker, G.; de Haas, M. P.; Siebbeles, L. D. A.; Warman, J. M. *Phys. Rev. B* **2004**, *70*, 045203.
(27) Hoofman, R. J. O. M.; de Haas, M. P.; Siebbeles, L. D. A.; Warman, J. M. *Nature* **1998**, *392*, 54−56.
(28) Warman, J. M.; Gelinck, J. H.; de Haas, M. P. *J. Phys.: Condens. Matter* **2002**, *14*, 9935−9954.
(29) Prins, P.; Grozema, F. C.; Galbrecht, F.; Scherf, U.; Siebbeles, L. D. A. *J. Phys. Chem. C* **2007**, *111*, 11104−11112.
(30) Prins, P.; Grozema, F. C.; Schins, J. M.; Siebbeles, L. D. A. *Phys. Status Solidi B* **2006**, *243*, 382−386.
(31) Bard, A. J.; Faulkner, L. R. *Electrochemical Methods: Fundamentals and Applications*; John Wiley & Sons, Inc.: New York, NY, 2001.
(32) Cardona, C. M.; Li, W.; Kaifer, A. E.; Stockdale, D.; Bazan, G. C. *Adv. Mater.* **2011**, *23*, 2367−2371.
(33) Dayal, S.; Kopidakis, N.; Rumbles, G. *Faraday Discuss.* **2012**, *155*, 323−337.

(34) Chua, L. L.; Zaumseil, J.; Chang, J. F.; Ou, E. C. W.; Ho, P. K. H.; Sirringhaus, H.; Friend, R. H. *Nature* **2005**, *434*, 194−199.

(35) Schueppel, R.; Uhrich, C.; Pfeiffer, M.; Leo, K.; Brier, E.; Reinold, E.; Baeuerle, P. *ChemPhysChem* **2007**, *8*, 1497−1503.

(36) Shoaee, S.; Clarke, T. M.; Huang, C.; Barlow, S.; Marder, S. R.; Heeney, M.; McCulloch, I.; Durrant, J. R. *J. Am. Chem. Soc.* **2010**, *132*, 12919−12926.

(37) Marcus, R. A. *J. Chem. Phys.* **1956**, *24*, 966−978.

(38) Closs, G. L.; Miller, J. R. *Science* **1988**, *240*, 440−447.

(39) Suppan, P. *Top. Curr. Chem.* **1992**, *163*, 95−130.

(40) Fukuzumi, S.; Ohkubo, K.; Imahori, H.; Guldi, D. M. *Chem.—Eur. J.* **2003**, *9*, 1585−1593.

(41) Angulo, G.; Rosspeintner, A.; Vauthey, E. *J. Phys. Chem. A* **2011**, *115*, 7858−7860.

(42) Chakraborty, A.; Chakrabarty, D.; Ham, P.; Seth, D.; Sarkar, N. *Chem. Phys. Lett.* **2004**, *387*, 517−517.

(43) Kumbhakar, M.; Nath, S.; Pal, H.; Sapre, A. V.; Mukherjee, T. *J. Chem. Phys.* **2003**, *119*, 388−399.

(44) Barbara, P. F.; Meyer, T. J.; Ratner, M. A. *J. Phys. Chem.* **1996**, *100*, 13148−13168.

(45) Koster, L. J. A.; Shaheen, S. E.; Hummelen, J. C. *Adv. Energy Mat.* DOI: 10.1002/aenm.201100523.

8923

dx.doi.org/10.1021/jp302275z | *J. Phys. Chem. C* 2012, 116, 8916−8923